NASA Contractor Report 4116

A Vectorized Poisson Solver Over a Spherical Shell and Its Application to the Quasi-Geostrophic Omega-Equation

Paul Mullenmeister
Sigma Data Services
Rockville, Maryland

Prepared for
Goddard Space Flight Center
under Contract NAS5-20784

National Aeronautics
and Space Administration

**Scientific and Technical
Information Division**

1988

PREFACE:

A vectorized Poisson solver, specifically designed for the CDC 200 computer series, was developed to obtain solutions of self-adjoint differential equations of the type:

$$a(p)\ \nabla \cdot [b(\varphi,\lambda,p)\ \nabla u] + c(\varphi,\lambda)\ \partial^2_p u = source(\varphi,\lambda,p)$$

$$(\ \nabla := \nabla_{\varphi\lambda}\ )$$

where u is the unknown variable and a, b, c represent the coefficients as functions of the spatial variables φ, λ, p . The purpose of this solver is to generate solutions for large gridsizes with spherical geometry at a high efficiency rate. It is assumed that the radial extent of the physical domain is much smaller than its average distance from the center of the sphere.

The two-parameter Chebyshev method has desirable properties such as an effective convergence rate and simple implementation for vector processors. The algorithm can be applied to a variety of problems with spherical geometry.

It allows to obtain solutions of the quasi-geostrophic omega-equation if its coefficients are spatially distributed such that the equation remains elliptic. A three-month GCM simulation provides the data base for the computation of the quasi-geostrophic omega solution which is verfied against the fields obtained from the divergent wind fields.

The results presented in this publication are part of a more extensive diagnostic study of the mechanisms responsible for the maintenance of the general circulation.

TABLE OF CONTENTS

1. Introduction..... 1

2. Formulation of the quasi-geostrophic omega-equation.. 2

3. Finite Difference Form of the omega-equation..... 5

4. Design of a vectorized Poisson algorithm for CDC 200. series..... 9

5. Example of an application of the vectorized Poisson.. solver and discussion of results.....13

5.1 Observed and GLAS-GCM omega fields.....13

5.2 Quasi-geostrophic omega field from GCM data.....14

6. Acknowledgements.....16

7. References.....17

8. Appendix: Sample figures.....18

1. INTRODUCTION

The development of a vectorized Poisson solver was motivated by the need to obtain solutions of the quasi--geostrophic omega-equation.

With the aid of the quasi-geostrophic omega-equation the driving forces of the general circulation can be examined individually since partial solutions of the omega-equation are obtainable as response to individual source terms. Therefore the relative roles of dynamical and physical processes and orography in producing the vertical velocity distribution can be ascertained.

Primitive equation models provide a nonlinear omega from the mass continuity equation using the divergent wind fields. The "primitive" omega is more accurate, and to the extent that quasi-geostrophic theory is valid, compares with the linear quasi-geostrophic omega. The effort to calculate the quasi-geostrophic omega is much greater, and thus requires the development of an efficient three-dimensional Poisson solver which is applied to a spherical grid of 72 x 46 x 9 gridpoints.

In Section 2, we express the analytic form of the omega-equation in flux form to facilitate the application of a suitable finite difference scheme. The physical domain is geometrically a spherical shell with large radius. In Section 3, the finite difference equations are developed, using the box method which preserves symmetry of the finite difference equations. Section 4 describes the vector layout of a point Chebyshev solver for CDC 200 series computers. The convergence rate is accelerated by the choice of two iteration parameters which are functions of the spectral radius of the iteration matrix. In Section 5, we present a discussion of some results from a three-month integration of the GLA Fourth-Order General Circulation Model (see Kalnay et al., 1983). It includes a comparison of the "primitive" model omega field and the recalculated quasi-geostrophic omega field, which are verfied against the observed "primitive" omega from FGGE III b data.

2. FORMULATION OF THE QUASI-GEOSTROPHIC OMEGA-EQUATION

The vorticity, divergence, thermodynamic, and continuity equations describing the linear balanced model are:

$$\partial_t \nabla^2 \psi + \mathbf{v}_\psi \cdot \nabla(\xi+f) + \mathbf{v}_\chi \cdot \nabla f = f\partial_p \omega \tag{2.1}$$

$$f\nabla^2 \psi + \nabla f \cdot \nabla \psi = \nabla^2 \Phi \tag{2.2}$$

$$\partial_t \partial_p \Phi + \mathbf{v} \cdot \nabla \partial_p \Phi + \sigma\omega = -Q \tag{2.3}$$

$$\nabla^2 \chi + \partial_p \omega = 0 \tag{2.4}$$

where Q denotes the sum of all heating terms and σ represents the static stability parameter (see Haltiner and Williams, 1980).

Upon multiplying (2.1) by f and introducing (2.2) into (2.1), the vorticity equation becomes:

$$\partial_t \nabla^2 \Phi - \nabla f \cdot \nabla \partial_t \psi + f\mathbf{v}_\psi \cdot \nabla(\xi+f) + f\mathbf{v}_\chi \cdot \nabla f = f^2 \partial_p \omega \tag{2.5}$$

Upon eliminating time derivatives between equations (2.3) and (2.5) [with the aid of (2.2)] one obtains the omega-equation:

$$\nabla^2(\sigma\omega) + f^2 \partial^2{}_p \omega = f\partial_p [\mathbf{v}_\psi \cdot \nabla(\xi+f)] - \nabla^2(\mathbf{v} \cdot \nabla \partial_p \Phi) - \nabla^2 Q + f\nabla f \cdot \partial_p \mathbf{v}_\chi - \nabla f \cdot \nabla \partial_p \partial_t \psi \tag{2.6}$$

It takes the form of the quasi-geostrophic omega-equation if one neglects the last term in the foregoing relationship. By virtue of scale analysis this term can be shown

to be negligible compared with the differential vorticity advection in midlatitudes and compared with the heating in the tropics.

Without introducing any sensible error we may also add the small term $f\partial_p(\mathbf{v}_\chi \cdot \nabla\xi)$ which [with the neglect of the last term in (2.6)] enables us to write (2.6) in the form:

$$\nabla^2(\sigma\omega) + f^2\partial^2{}_p\omega = f\partial_p[\mathbf{v} \cdot \nabla(\xi+f)] - \nabla^2[\mathbf{v} \cdot \nabla(\partial_p\Phi+Q)] \tag{2.7}$$

which is desirable for reasons of computational simplicity.

The parameters σ and f slowly vary over the globe. Following Hoskins (1978) we may treat the static stability parameter as a constant over length scales of the order of the Rossby radius and smaller, but as varying over larger scales. To ensure the latter assumption, the static stability is computed as an equally-weighted nine point horizontal average in space. It is therefore a function of all three spatial variables whereas the Coriolis parameter naturally depends on φ only. As a result, the elliptic omega-equation can be approximated with little error in flux form:

$$\begin{aligned}
&\partial_\lambda(\alpha/\theta\ \Gamma\ \partial_\lambda\omega) + \cos\varphi\ \partial_\varphi(\cos\varphi\ \alpha/\theta\ \Gamma\ \partial_\varphi\omega) \\
&\qquad + r^2\cos^2\varphi\partial_p(f^2\partial_p\omega) \\
&= f\ r\ \cos\varphi\ \partial_p[u\ \partial_\lambda(\xi+f)] + f\ r\ \cos^2\varphi\ \partial_p[v\ \partial_\varphi(\xi+f)] \\
&+ \alpha/\theta\ [\partial^2{}_\lambda + \cos\varphi\ \partial_\varphi(\cos\varphi\partial_\varphi)] \\
&\qquad [u/(r\ \cos\varphi)\ \partial_\lambda\theta + v/r\ \partial_\varphi\theta] \\
&- \alpha/\theta\ [\partial^2{}_\lambda + \cos\varphi\ \partial_\varphi(\cos\varphi\partial_\varphi)]\ Q
\end{aligned} \tag{2.8}$$

where $\Gamma = -\partial_p \theta$ denotes the static stability.

The equation can be rewritten concisely as:

$$L_\omega(\omega) := <(\nabla, \partial_p), (\alpha/\theta\ \Gamma\ \nabla, f^2 \partial_p) > \omega$$

$$= f\ \partial_p(\mathbf{v} \cdot \nabla(\xi+f) + \alpha/\theta\ \nabla^2(\mathbf{v} \cdot \nabla\theta - Q^*) \qquad (2.9)$$

where $Q^* = \theta/\alpha\ Q$ and $< \mathbf{a}\ ,\ \mathbf{b} >$ denotes the scalar product of $\mathbf{a}$ and $\mathbf{b}$. In this form, it becomes apparent that the associated operator L_ω is self-adjoint in an integral sense with respect to the weighting function $1/(\alpha/\theta\ \Gamma\ f^2)$.

The boundary conditions at the bottom and the top of the atmosphere are given by the expressions

$$\omega = -\rho_s \mathbf{v}_s \cdot \nabla(\Phi_s - \Phi)$$

(where for our climatological analysis $\mathbf{v}_s \cdot \nabla\Phi$ is neglected in consistence with our quasi-geostrophic assumption), and

$\omega = 0$, respectively.

3. FINITE DIFFERENCE FORM OF THE OMEGA-EQUATION

Above formulation of the partial differential equation in flux form allows symmetric finite difference equations although the grid need not be uniform. This greatly reduces storage as shall be elucidated in this and the following section.

Equation (2.9) of Section 2 is integrated at each mesh- point over a box with the meshpoint at its center:

$$\iiint_V (\nabla, \partial_p) \cdot (\alpha/\theta \; \Gamma \; \nabla, f^2 \; \partial_p) \; \omega \; dV = \iint_{S(V)} (\alpha/\theta \; \Gamma \; \nabla\omega, f^2 \partial_p \omega) \cdot dS$$

$$= \iiint_V RHS \; dV \qquad (3.1)$$

where RHS represents the right-hand-side of (2.9) and the volume integral of the left-hand-side has been converted into a surface integral with S the surface of volume element V .

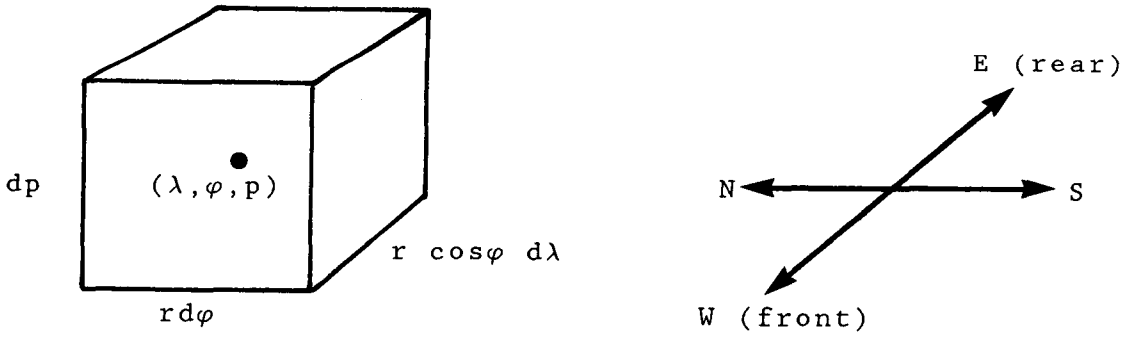

Figure 1: geometric configuration

The volume element is given by $dV = r^2 \cos\varphi \, d\varphi \, d\lambda \, dp$ and the surface elements of the faces are:

$r \cos\varphi \, d\lambda \, dp$ in the South-North (S-N) direction

$r^2 \cos\varphi \, d\lambda \, d\varphi$ in the bottom-top direction

$r \, d\varphi \, dp$ in the West-East (W-E) direction

To obtain the finite difference equations, we introduce the indices i, j, and k denoting W-E, S-N, and bottom-top directions running from 1 to I, 1 to J, and 1 to K respectively. Thus, we obtain:

$$\iiint_V \text{RHS} \; dV = \text{RHS}_c \; r^2 \cos^2\varphi_c \; \Delta\lambda \; \Delta\varphi \; \Delta p \qquad (3.2)$$

and the different face contributions to the coefficients from the surface integral are:

upper face: $f^2 \; (\omega_{k+1} - \omega_k)/(p_{k+1} - p_k) \; r^2 \cos^2\varphi_c \; \Delta\varphi \; \Delta\lambda$

lower face: $f^2 \; (\omega_{k-1} - \omega_k)/(p_k - p_{k-1}) \; r^2 \cos^2\varphi_c \; \Delta\varphi \; \Delta\lambda$

front face: $\sigma_{\text{front}} \; (\omega_{i-1} - \omega_i)/(r \cos\varphi_c \; \Delta\lambda) \; r \; \Delta\varphi \; \Delta p$

rear face: $\sigma_{\text{rear}} \; (\omega_{i+1} - \omega_i)/(r \cos\varphi_c \; \Delta\lambda) \; r \; \Delta\varphi \; \Delta p$

Northern face: $\sigma_N \; (\omega_{j+1} - \omega_j)/(r\Delta\varphi) \; r \cos\varphi_N \; \Delta\lambda \; \Delta p \cos\varphi_c$

Southern face: $\sigma_S \; (\omega_{j-1} - \omega_j)/(r\Delta\varphi) \; r \cos\varphi_S \; \Delta\lambda \; \Delta p \cos\varphi_c$

(3.3-3.8)

where subscripts c, S, N indicate evaluation of the corresponding variable at the center, the Southern face, the

Northern face of the volume element, respectively, and Δp is defined as:

$$1/2\ (p_{k+1}-p_{k-1}) \qquad \text{for interior nodes.}$$

σ_{front}, σ_{rear}, σ_N and σ_R are obtained by linear interpolation from neighboring meshpoints.

In finite difference form, the source terms and LHS omega terms are computed consistently with order(distance) truncation error. Periodic boundary conditions are specified in the East-West direction, Dirichlet conditions at the bottom and top of the atmosphere which are assumed to be at 1000mb and 50mb.

The kinematic condition at the bottom expands to:

$$\omega = -p_s/RT_s\{u/(r\ \cos\varphi)\ \partial_\lambda \Phi_s + v/r\ \partial_\varphi \Phi_s\} \qquad (3.9)$$

The grid is treated as a rectangle with multiple representation of the North and South poles. Half-box geometry is applied along the six boundary planes. The coefficients across the boundary faces of these half-boxes are taken to be zero (zero-flow condition).

The periodicity condition along the meridian boundary at 180° longitude East and West is achieved by adapting the following procedure:

Half-box geometry factors are applied at both boundaries (180° West, 180° East) to obtain the coefficients. During each iteration the two separate corresponding solutions pertaining to the half-boxes are arithmetically combined to form a single solution (see algorithm in Section 4).

The spatially symmetric formulation of the finite difference equation requires only storage of four coefficient sets: a set of diagonal coefficients and one set for each geometric direction. These coefficients are specified on a three dimensional grid with index i starting at 180° West, index j starting at the South pole, and index k starting at the bottom of the atmosphere.

assigning a large number, say 10^{12}, to the diagonal coefficient of those meshpoints on the boundary and outside the physical domain. Correspondingly, the RHS must be specified as the product of the unknown variable ω and this pre-set large number on the boundary.

4. DESIGN OF A VECTORIZED POISSON ALGORITHM FOR CDC 200 SERIES

It is important to select a suitable layout for indexing the arrays and a method which allows vectorization of the iteration scheme.

As pointed out in the foregoing section, special consideration must be given to the boundary nodes which include the polar nodes, the nodes at the top and bottom of the grid and the meridian boundary where the solution from both ends must be joined:

The adjacent longitudes outside the physical domain are occupied with a set of zero off-diagonal coefficients. This ensures vectorization of the entire code without the need for checking indices in any of the three geometric directions during the iteration process.

Six descriptors "D" for the six different directions and one descriptor for the center of the individual meshbox pointing to the proper addresses of the coefficient vectors are introduced:

```
D(CW) = D(CE) - 1

D(CS) = D(CN) - I

D(CB) = D(CA) - IJ

D(CP)
```

where CE/CW, CN/CS and CA/CB are three off-diagonal coefficient sets referring to the East, North, and top directions, CP the diagonal coefficient set and "D" descriptors pointing toward the proper locations.

Similarly, six descriptors plus an additional one are also needed for the solution vector of the unknown variable ω .

As iteration procedure, a point Chebyshev method with

adaptive determination is implemented because of its versatility and applicability for solutions of large three--dimensional elliptic equations. This iterative method can be ideally vectorized and is proved to be efficient for large 3D elliptic equations.

Two iteration parameters, alpha (α) and beta (β), need to be specified which are updated prior to each iteration step. The rate of convergence depends largely on the choice of these parameters. The fact that the number of vertical planes is much smaller than the number of planes in any of the two horizontal directions leads to rapid convergence. For the present problem, we select a spectral radius of 0.9 which detemines the coefficients of the Chebyshev recursion formulas for the iteration parameters:

$$\alpha(1) := 0.95238 \qquad \alpha(2) := 1.6123$$

$$\alpha(t) := 1. \; / \; [1.05 - 0.225625\, \alpha(t-1)] \quad \text{for } t>2$$

$$\beta(1) := 0.$$

$$\beta(t) := 1.05\, \alpha(t) - 1. \quad \text{for } t>1 \qquad (4.1)$$

With these choices, alpha approaches a value of approximately 1.336 and beta approaches a value of approximately 0.403 as t approaches infinity.

Upon defining UNOW as the solution vector, UM1 and UM2 as auxiliary iteration vectors, SOURCE as the RHS and CPINV as the vector of reciprocal diagonal coefficients, we can summarize the iteration algorithm in CDC Vector Fortran as follows:

```
UNOW = -SOURCE

t = 1
```

```
100 UNOW(i=1,j,k) = UNOW(i=I,j,k) replaced by
                    UNOW(i=1,j,k) + UNOW(i=I,j,k)
                    (to account for periodicity condition)
    UNOW = CPINV*UNOW
    UNOW = ALPHA(t)*(UNOW - UM1) + BETA(t)*(UM1 - UM2)
    USPOLE(k) = average over i of UNOW along line (j=1)
                for k=1,K
    UNPOLE(k) = average over i of UNOW along line (j=J)
                for k=1,K
    UM2  = UM1
    UM1  = UNOW + UM1
    UNOW = -SOURCE + CE*UM1E + CW*UM1W
                   + CN*UM1N + CS*UM1S
                   + CA*UM1A + CB*UM1B
    (where appended letters E, W... indicate addresses
    pertaining to the East, West... directions)
    t    = t + 1
    go to 100  (until convergence is reached)
```

UM1 and UNOW are periodically compared in order to terminate the iteration when sufficient accuracy is achieved.

To achieve an accuracy of 10^{-5} starting with the highest significant digit, approximately 300 iterations and 1-1.5 CPU seconds on a CDC 205 are needed for our applications to a grid with approxiamtely 40,000 gridpoints

and given source distribution (The value 40,000 is ideally below the critical limit for vector processing on the CDC 205, namely $2^{16} - 1 = 65,535$).

The vectorized algorithm is remarkably superior to its scalar, but otherwise identical analogue with a CPU performance of approximately 100 CPU seconds.

The above described algorithm is applicable to a wide variety of other Poisson problems with spherical geometry which, for example, frequently arise in the context of electrostatics and heat flow.

5. EXAMPLE OF AN APPLICATION OF THE VECTORIZED POISSON AND DISCUSSION OF RESULTS

5.1 Observed and GLAS-GCM omega fields

Figure A1 shows a three month average of the 500mb vertical velocity (omega) field for the period from Dec 15, 1978 to Mar 15, 1979, calculated by Krishnamurti and Sheng (1984) from unitialized ECMWF FGGE IIIb divergent wind field patterns. Bands of rising motion (unshaded areas) are clearly centered near the equator and sixty degrees North and South latitude with bands of sinking motion centered around thirty degrees North and South. An intense center of sinking motion is found on the southern slope of the Himalayas north of the Bay of Bengal. Another prominent feature is the center of rising motion extending south-eastward from South America almost connecting with the ascending belt around sixty degrees South. There is also an intricate vertical motion pattern with rising motion across the Andes.

Figure A2 shows the corresponding vertical motion pattern derived from a GLAS three-month simulation using the formula

$$\omega = \dot{\sigma}\pi + \sigma\dot{\pi} \qquad (5.1)$$

where $\dot{\sigma}$ is the vertical velocity in σ - coordinates, obtained from divergent wind field pattern, and π is the surface pressure. This field is interpolated from the model grid to a pressure coordinate system and then to the FGGE horizontal grid by means of bicubic splines. As in the case of the vertical motions derived from the ECMWF FGGE IIIb analysis, the simulated vertical velocity pattern exhibits bands of sinking motion in the proximity of thirty degrees North and South. It also displays a band of rising motion extending SE from Brazil to the rising band at sixty degrees South. The smaller scale centers of vertical motion are, however, more intense than those of Figure A1 and do not correlate well with the latter. The corre-

lation coefficient between the area-weighted omega fields at 500mb shown in Figures A1 and A2 is in fact only 0.27 + 0.03, which means that the simulated field accounts for only about 9% of the variance of the analyzed field.

A notable feature of the simulated field is the bimodal distribution of vertical motion associated with each of the major mountain chains, with East-West orientation in the case of the Rocky Mountains, the Himalayas and the Andes, and a North-South orientation in the case of the Greenland Plateau. (The GLAS enhanced topography field is shown in Figure A3.) The vertical motion pattern in the vicinity of the Andes is more complicated than in the FGGE analysis. There is also a prominent region of the upward motion in equatorial East Africa which has no counterpart in the FGGE analysis.

5.2 Quasi-geostrophic omega field from GCM data

In order to investigate the features of the GLAS simulated model omega we solved equation (2.9) with the aid of the vectorized Poisson solver to obtain the quasi--geostrophic vertical velocity field. Scale analysis of the most general form of the omega-equation reveals that the quasi-geostrophic version is valid in middle and high latitudes where the Rossby number is small. The same analysis reveals that near the equator the dominant terms are $\nabla\Gamma \cdot \nabla\omega$ and Q, with all other terms being negligible. Since the quasi-geostrophic omega equation also reduces to a balance between these two terms as the equator is approached, we shall use it rather than the more general omega-equation arising from the balance equation which is more cumbersome to solve.

To the extent that the quasi-geostrophic omega--equation is valid and friction forcing has a negligble effect on the vertical motion at 500mb, the solution of equation (2.9) forced by the sum of all other forcing terms on the right should resemble the omega field obtained from the GLAS model simulation. Figure A4 reveals that it does, although the maxima and minima are somewhat weaker than

those in the original simulation. Figure A4 was obtained by time-averaging the individual solutions of the omega--equation at 181 twelve-hour intervals from 00Z Dec 15, 1978 through 00Z Mar 15, 1979. This is necessary in principle because static stability, which appears as a coefficient on the LHS of the omega-equation, varies with time and could conceivably correlate with ω .

6. ACKNOWLEDGEMENTS

The author would like to express his gratitude to Professors Richard Pfeffer, Florida State University and Eugene Washpress, University of Tennessee and CDC Consultant, for their suggestions and advice.

7. REFERENCES

Haltiner, G. J. and R. T. Williams, 1980: Numerical Weather Prediction and Dynamica Meteorology, John Wiley & Sons, Chapter 7.

Hoskins, B.J., I. Draghici, and H.C. Davies, 1978: A new look at the omega-equation. Quart. J. R. Met. Soc., 104, 31-38.

Kalnay, E., R. Balgovind, W. Chao, D. Edelmann, J. Pfaendtner, L. Takacs, and K. Takano, 1983: Documentation of the GLAS fourth-order general circulation model. NASA Technical Memorandum 86064, Greenbelt, MD 20771.

Krishnamurti, T.N. and C. Sheng, 1984: Vertical velocities recalculated for the FGGE year. Unpublished documentation.

Lu, H.I. and R.L. Pfeffer, 1985: Application of the spectral method to solve the meridional circulation equation in spherical sigma coordinates. Mon. Wea. Rev., 113, 1868-1875.

Meis, Th. and U. Marcowitz, 1978: Numerische Behandlung partieller Differentialgleichungen. Springer-Verlag Berlin, Kapitel 3.

Mullenmeister, P., 1986: Analyses of short-term and long-term forecasting experiments using the GLAS-GCM. Master's Thesis, Florida State University.

Pfeffer, R.L., 1981: Wave-mean flow interactions in the atmosphere. J. Atmos. Sci., 38, 1340-1359.

Washpress, E.L., 1966: Iterative solutions of elliptic systems. Prentice Hall, Englewood, New Jersey.

8. APPENDIX

The following figures referenced in the text show the observed FGGE omega field at 500mb, (Figure A1), the GLAS--GCM model omega field (Figure A2), the bottom topography (Figure A3), and the quasi-geostrophic omega field (Figure A4).

The contour interval in Figures A1, A2 and A4 is:

$$0.5\ 10^{-3}\ \text{mb/s}.$$

The contour interval in Figure A3 is:

$$0.5\ 10^{4}\ \text{m}^2/\text{s}^2.$$

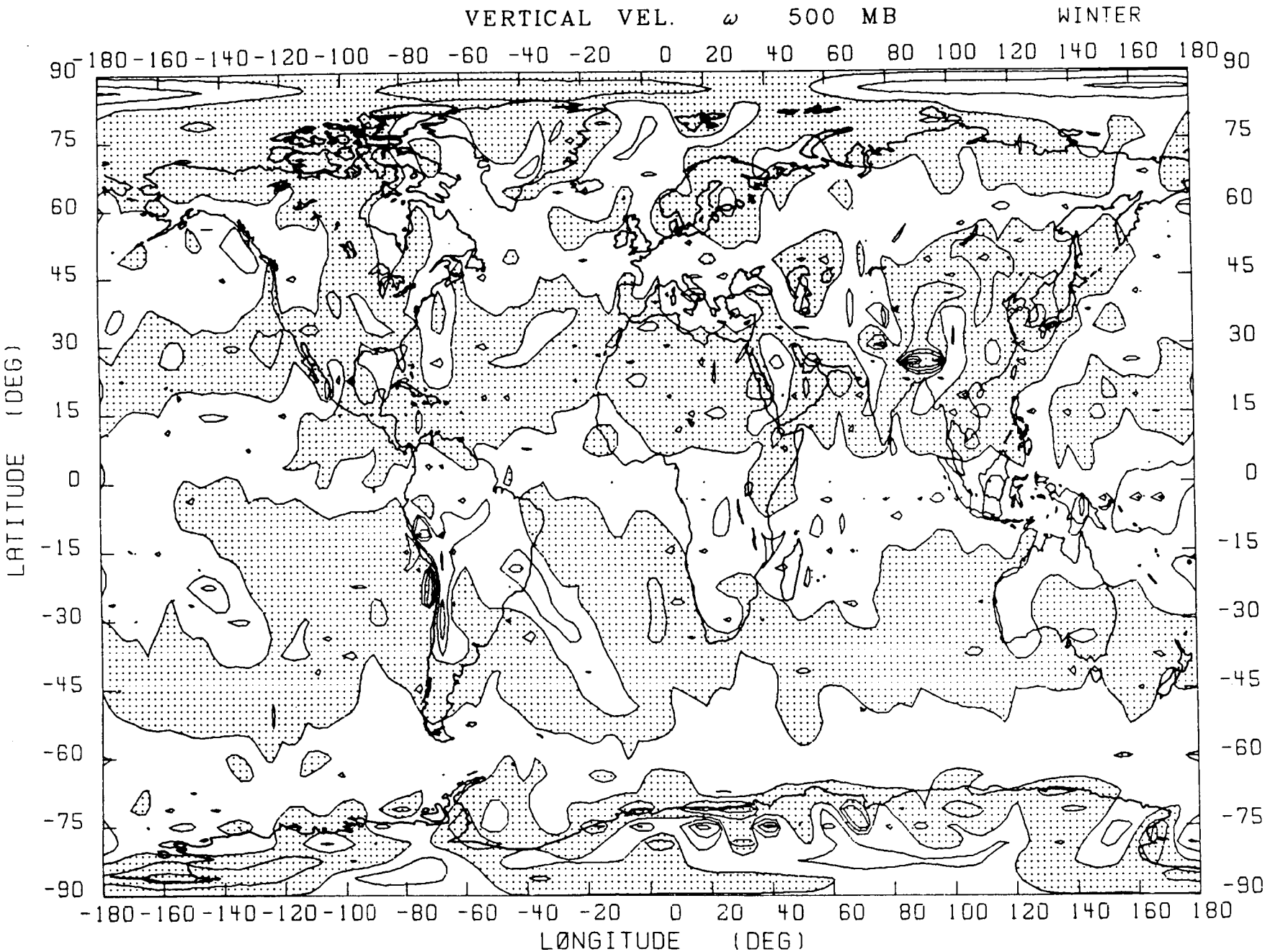
VERTICAL VEL. ω 500 MB WINTER
-180 -160 -140 -120 -100 -80 -60 -40 -20 0 20 40 60 80 100 120 140 160 180
90 75 60 45 30 15 0 -15 -30 -45 -60 -75 -90
LATITUDE (DEG)
LØNGITUDE (DEG)

Figure A1

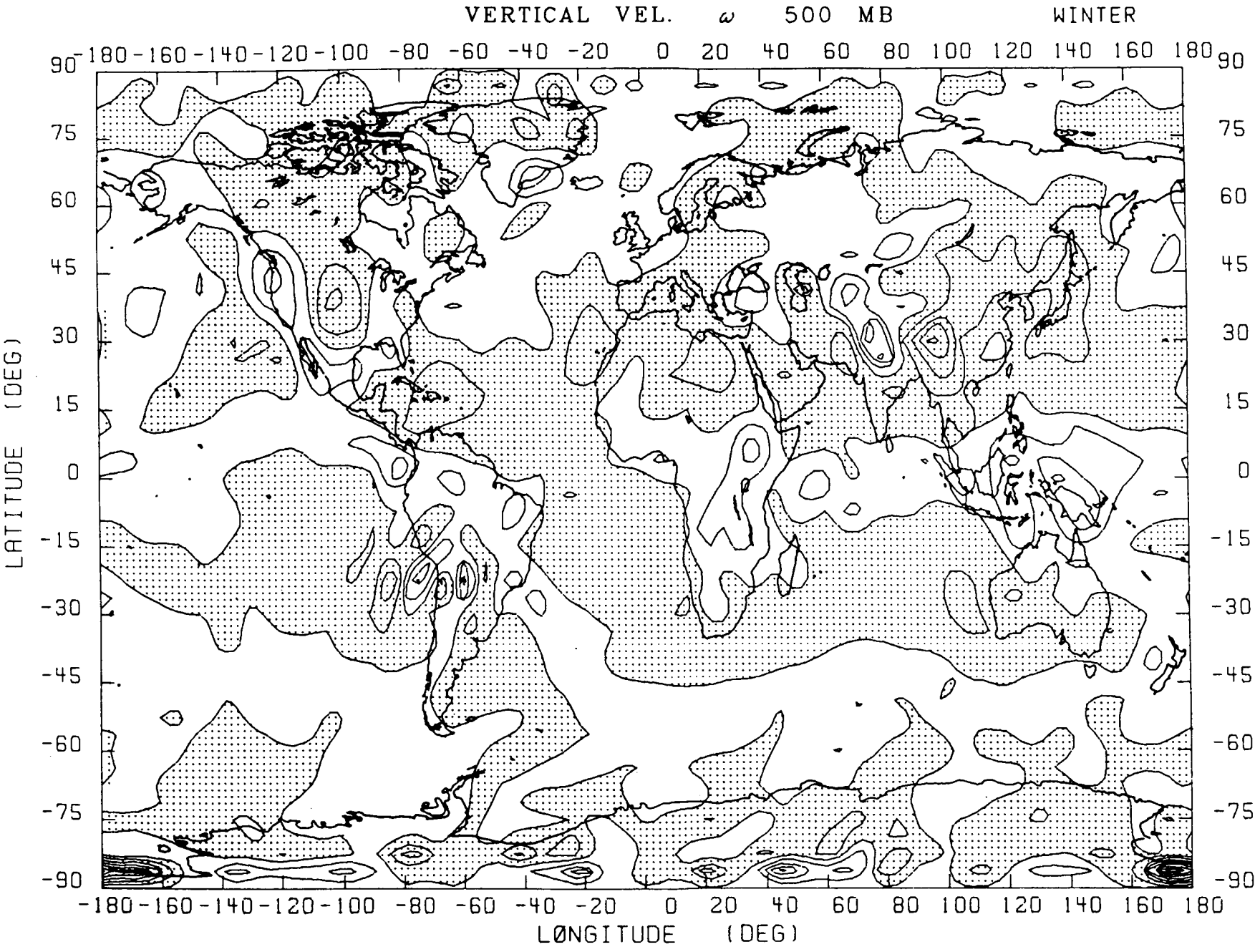
VERTICAL VEL. ω 500 MB WINTER
-180 -160 -140 -120 -100 -80 -60 -40 -20 0 20 40 60 80 100 120 140 160 180
90 75 60 45 30 15 0 -15 -30 -45 -60 -75 -90
LATITUDE (DEG)
LONGITUDE (DEG)

Figure A2

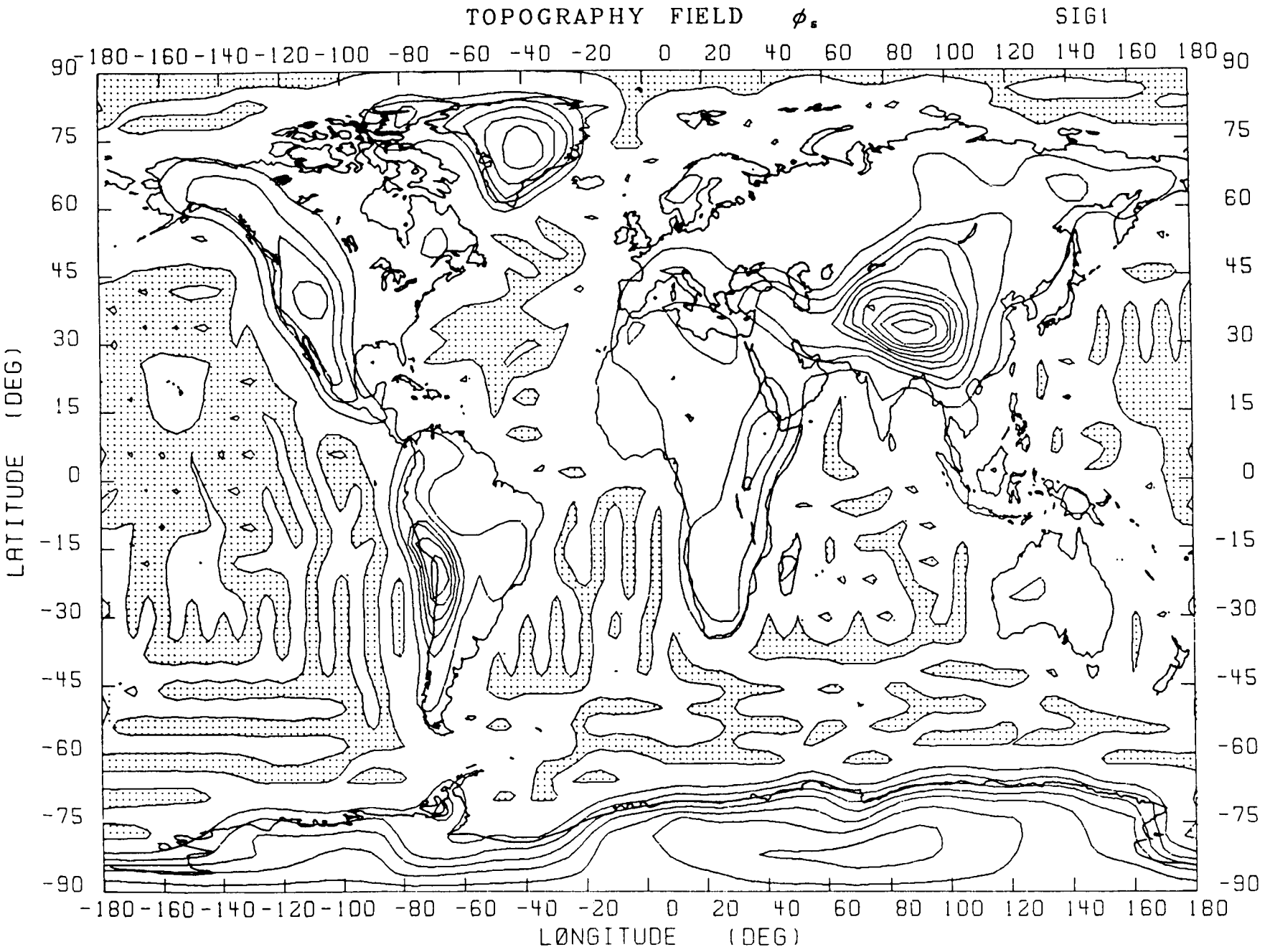
TOPOGRAPHY FIELD ϕ_s
SIG1
-180 -160 -140 -120 -100 -80 -60 -40 -20 0 20 40 60 80 100 120 140 160 180
90 75 60 45 30 15 0 -15 -30 -45 -60 -75 -90
LATITUDE (DEG)
LONGITUDE (DEG)

Figure A3

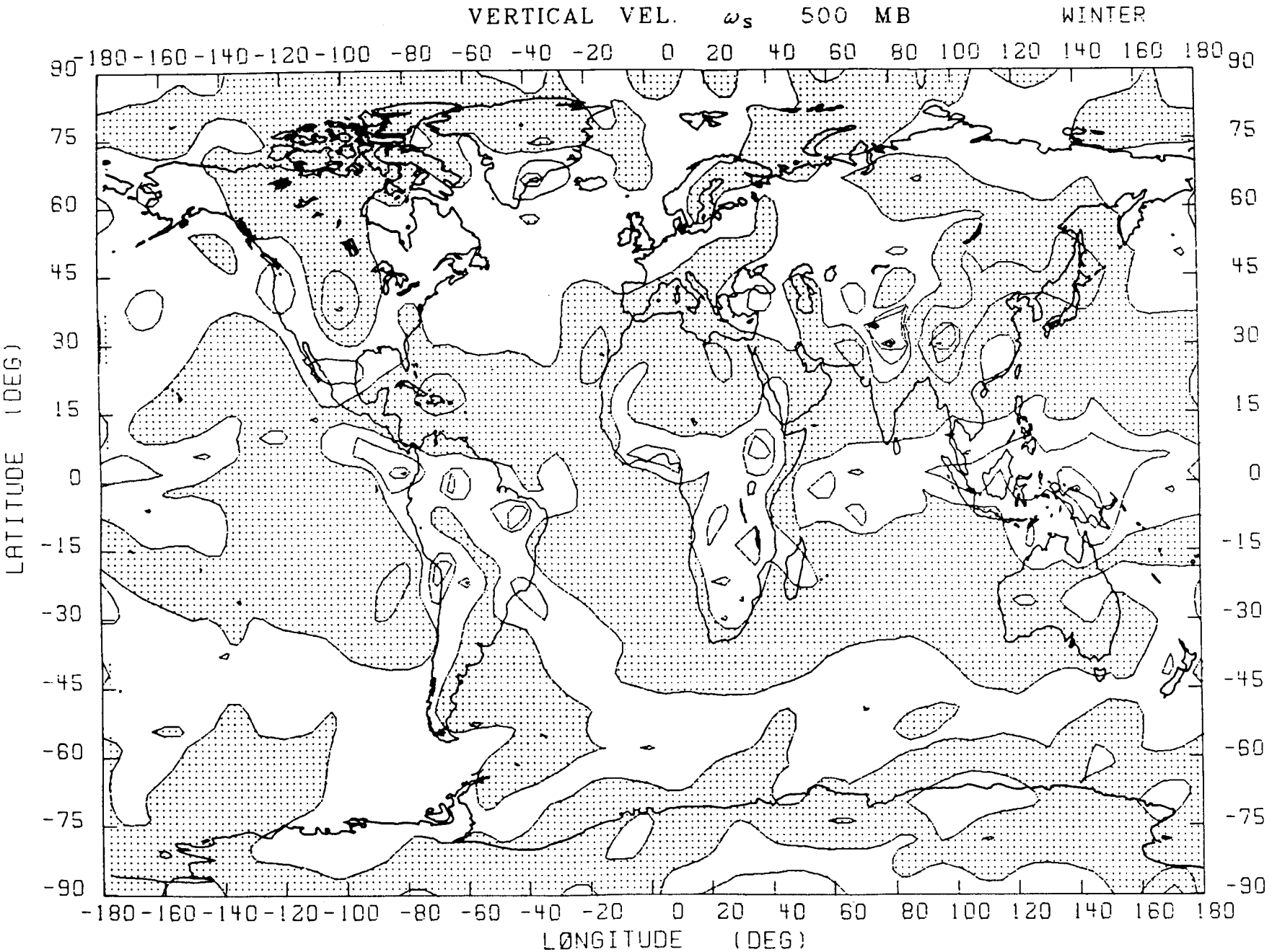
VERTICAL VEL. ω_s 500 MB WINTER
-180 -160 -140 -120 -100 -80 -60 -40 -20 0 20 40 60 80 100 120 140 160 180
90 75 60 45 30 15 0 -15 -30 -45 -60 -75 -90
LATITUDE (DEG)
LONGITUDE (DEG)

Figure A4

NASA
National Aeronautics and Space Administration

Report Documentation Page

1. Report No.	2. Government Accession No.	3. Recipient's Catalog No.
NASA CR-4116		

4. Title and Subtitle
A Vectorized Poisson Solver Over a Spherical Shell and Its Application to the Quasi-Geostrophic Omega-Equation

5. Report Date
February 1988

6. Performing Organization Code

7. Author(s)
Paul Mullenmeister

8. Performing Organization Report No.
87B1000

10. Work Unit No.

9. Performing Organization Name and Address
Sigma Data Services
6011 Executive Boulevard, Suite 300
Rockville, Maryland 20852

11. Contract or Grant No.
NAS5-20784

13. Type of Report and Period Covered
Contractor Report

12. Sponsoring Agency Name and Address
National Aeronautics and Space Administration
Washington, D.C. 20546-0001

14. Sponsoring Agency Code

15. Supplementary Notes
Mr. Mullenmeister is affiliated with Sigma Data Services; Rockville, Maryland; 20852.

16. Abstract
The quasi-geostrophic omega-equation in flux form is developed as an example of a Poisson problem over a spherical shell. Solutions of this equation are obtained by applying a two-parameter Chebyshev solver in vector layout for CDC 200 series computers.

The performance of this vectorized algorithm greatly exceeds the performance of its scalar analogue.

The algorithm generates solutions of the omega-equation which are compared with the omega fields calculated with the aid of the mass continuity equation.

17. Key Words (Suggested by Author(s))	18. Distribution Statement
Poisson solver for quasi-geostrophic omega-equation Two-parameter Chebyshev method CDC 200 vector layout	Unclassified-Unlimited Subject Category 47

19. Security Classif. (of this report)	20. Security Classif. (of this page)	21. No. of pages	22. Price
Unclassified	Unclassified	30	A04

NASA FORM 1626 OCT 86